Iterative spectral method for solving electrostatic or magnetostatic problems in complex and evolving heterostructures

Tian-Le Cheng and You-Hai Wen

Phys. Rev. E **91**, 053307 — Published 22 May 2015

DOI: 10.1103/PhysRevE.91.053307

Efficient algorithm for solving electrostatic/magnetostatic problems in complex and evolving heterostructures

Tian-Le Cheng* and You-Hai Wen*

National Energy Technology Laboratory, 1450 Queen Ave S.W., Albany, OR 97321, USA

ABSTRACT Electrostatic/magnetostatic problems involving complex heterogeneity are nontrivial for modeling and simulation. Most existing numerical methods focus on sharp interface models and the computational cost increases with increasing complexity of the geometry. Here we develop an iterative spectral method, so-called bound charge successive approximation algorithm, to solve electrostatic/magnetostatic heterogeneity problems in the context of diffuse-interface modeling. As tests and verifications, this algorithm is applied to calculation of the depolarization factor of an ellipsoid, and simulation of random dielectric mixtures and the dielectophoretic motion of multiple particles. The algorithm shows excellent efficiency and the computational cost mainly depends on the permittivity/permeability contrast in the whole system, regardless of the complexity of the geometry. In particular, for evolving heterostructures the solution of bound charge in one time step can be used as input for the next, which could further significantly shorten the iteration (approximation) process, making it practical to simulate the long range electrostatic/magnetostatic interaction in complex and evolving heterostructures.

PACS numbers: 02.60.-x 41.20.Cv 73.40.-c 75.70.Cn

I. Introduction

Calculation of the long range electrostatic interaction in a materials system can be computationally very expensive. For dielectric materials, continuum or coarse-grained numerical models often use the dielectric constant to characterize the medium, which avoids direct calculation of the all-atom charge interactions, as the macroscopic dielectric constant is linked to the atomic polarizability, e.g., through the Clausius-Mossotti relation [1]. However, dielectric heterostructure is yet ubiquitous in ceramics due to imperfections such as micropores/cracks, in composites due to the presence of inclusions/fillers, and in soft matter such as colloid systems [2-

5] and biological materials [6-11]. Much effort has been devoted to evaluate the effective dielectric constant (EDC) of a dielectric mixture [12-14]. Despite the extensive studies on the effective medium theory, for a random complex dielectric heterostructure its EDC cannot be predicted by a general theory with satisfactory accuracy [15]. In addition, if the microstructural evolution is affected by the electric field then the inhomogeneous dielectric constant needs to be explicitly modeled to account for the local electric field effect, for a typical example, during dielectrophoresis (DEP) of multiple particles [4]. There has also been much effort for numerical solutions of the heterogeneity problems, such as finite element method [16-19], boundary element method [12, 20-22], immersed interface method [23], and variational approaches [24-29]. Existing numerical methods, however, mostly focus on the sharp-interface models in which the computational cost strongly relies on the complexity of geometry/microstructure. Efficiently modeling complex and especially evolving dielectric heterostructures is yet very challenging. Similar problems also exist for magnetic heterostructures, such as in a random magnetic composite [30], and in magnetophoresis [31]. In this paper we develop a novel bound charge successive approximation (BCSA) algorithm to solve the heterogeneity problems in the context of diffuse-interface/phase-field modeling [32, 33]. By taking the advantage of diffuse-interface models in capturing microstructural evolution in materials, and with application of the Fast Fourier Transform technique (FFT), the BCSA algorithm shows excellent performance in simulating the complex and/or evolving heterostructures.

II. Formulation

For electrostatic problems involving heterogeneous media, the governing equation is the Gauss's law for dielectrics,

$$\nabla \cdot [\varepsilon_r(\mathbf{r})\varepsilon_0 \mathbf{E}(\mathbf{r})] = \rho_f(\mathbf{r}), \tag{0}$$

where ε_0 is the free space permittivity, $\varepsilon_r(\mathbf{r})$ the local relative permittivity, $\mathbf{E}(\mathbf{r})$ electric field, and $\rho_f(\mathbf{r})$ the free charge density. Note that for electrostatics $\mathbf{E}(\mathbf{r})$ can be expressed as $\mathbf{E}(\mathbf{r}) = -\nabla\varphi(\mathbf{r})$ where φ is the electrostatic potential, thus Eq. (1) is equivalent to the general form of Poisson's equation, i.e., $\nabla \cdot [\varepsilon_r(\mathbf{r})\varepsilon_0 \nabla\phi(\mathbf{r})] + \rho_f(\mathbf{r}) = 0$. Alternatively, Eq. (1) can be rewritten as

$$\nabla \cdot [\varepsilon_0 \mathbf{E}(\mathbf{r})] = \rho(\mathbf{r}) \tag{0}$$

where the total charge density $\rho(\mathbf{r}) = \rho_f(\mathbf{r}) + \rho_b(\mathbf{r})$, and the bound charge density

$$\rho_b(\mathbf{r}) = -\nabla \cdot \mathbf{P}(\mathbf{r}), \tag{0}$$

also called polarization charge density or induced charge density in the literature, is coupled with the electric field. Commonly one considers linear dielectric materials so that

$$\mathbf{P}(\mathbf{r}) = \varepsilon_0 \chi(\mathbf{r}) \mathbf{E}(\mathbf{r}) \tag{0}$$

where $\chi(\mathbf{r}) = \varepsilon_r(\mathbf{r}) - 1$ is the local dielectric susceptibility. Equation (4) is the constitutive equation of the dielectric material. When the total charge density is given, the electric field can be directly solved by the spectral method which is frequently used in diffuse-interface/phase-field models [34-36],

$$\mathbf{E}(\mathbf{r}) = \mathbf{E}^{ex}(\mathbf{r}) - \frac{i}{\varepsilon_0} \int \frac{d^3k}{(2\pi)^3} \frac{\tilde{\rho}(\mathbf{k})}{k} \mathbf{n} e^{i\mathbf{k}\cdot\mathbf{r}}, \tag{0}$$

where $\mathbf{E}^{ex}$ can be any divergence-free external field known in advance (i.e., independent of the object charge system), i the imaginary unit, k the length of reciprocal space vector $\mathbf{k}$, $\mathbf{n} = \mathbf{k}/k$, and the tilde '~' of $\tilde{\rho}(\mathbf{k})$ indicates the Fourier Transform (FT) of total charge density $\rho(\mathbf{r})$ (same for the following symbols). Equation (5), conforming to Eq. (2), is equivalent to $\mathbf{E}(\mathbf{r}) = \mathbf{E}^{ex} + \frac{1}{4\pi\varepsilon_0} \int \frac{\rho(\mathbf{r}')(\mathbf{r} - \mathbf{r}')}{|\mathbf{r} - \mathbf{r}'|^3} d^3r'$ that is a result of the free space Coulomb's law (in this case, the effect of dielectric heterostructure is reflected by the bound charge). Therefore, given the charge distribution, the electric field can be solved efficiently just by invoking twice the FFT operations (forward and backward) [34, 36]. Note that for applying FFT, periodic boundary condition has to be enforced. However, the problem is that the bound charge density itself is yet part of solution.

Here we discuss in the context of diffuse-interface models in which all field variables are typically defined on regular grid points, and the field variables (including the so-called order parameters) transit smoothly across interfaces [32, 33]. In contrast to sharp-interface models, there is no abrupt change of field variables across a diffuse interface. In the classical Cahn-Hilliard model that is based on the theory of gradient thermodynamics, the equilibrium profile of an order parameter across an interface is typically a hyperbolic tangent function [37]. In this

work, the dielectric susceptibility is also assumed to smoothly transit from 0 to $\varepsilon_r^0 - 1$ across a few grid points (the diffuse interface). See Fig. 1 for a schematic of a circular particle. The profile of χ across an interface is numerically treated to be approximately a smooth hyperbolic tangent function (other function could be used) so that the gradient of χ is not singular at the interfaces.

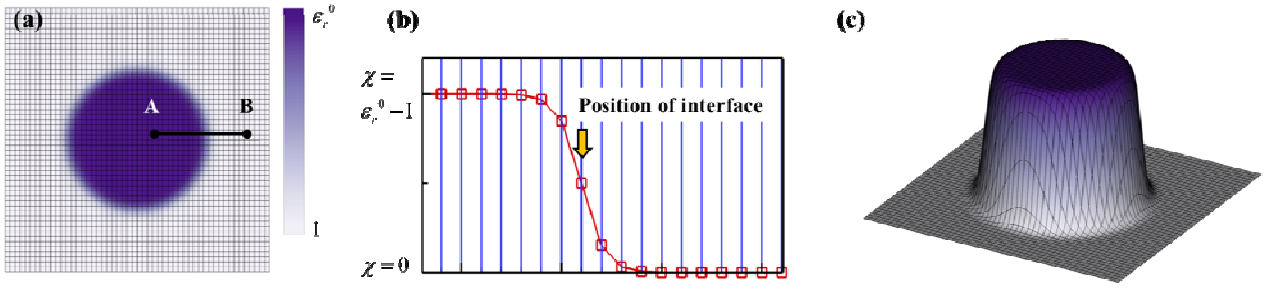

FIG. 1. (Color online) (a) schematic of a circular particle in vacuum modeled by diffuse-interface approach (the color denotes relative permittivity); (b) distribution of $\chi(\mathbf{r})$ along the path A-B in (a); (c) 3D visualization of the permittivity (set as height) and mesh in (a).

Combination of Eqs. (2-4) yields

$$\rho_b(\mathbf{r}) = \frac{-\varepsilon_0}{1+\chi(\mathbf{r})}\nabla\chi(\mathbf{r})\cdot\mathbf{E}(\mathbf{r}) - \frac{\chi(\mathbf{r})}{1+\chi(\mathbf{r})}\rho_f(\mathbf{r}). \tag{0}$$

It is clear that the uncertain part of the bound charge is just the first term of the right hand side of Eq. (6), since the last term consists of only predefined terms. We propose a straightforward method that we call a bound charge successive approximation algorithm (BCSA), to approach the bound charge solution step by step. The idea is to calculate the electric field by Eq. (5) first where the total charge density is set as the free charge density plus a tentatively evaluated bound charge density. Subsequently, the bound charge density is corrected according to the difference between the tentatively bound charge density and the value calculated from Eqs. (3-4). The corrected value is used as input for the next iteration step. This procedure is repeated until a convergence criterion is satisfied. At the *n*th iteration step (*n* starts from zero), the numerical operations are listed in Algorithm 1.

Algorithm 1: Bound Charge Successive Approximation (BCSA) algorithm for electrostatics

(a) $\rho^{(n)} = \rho_b{}^{(n)} + \rho_f$; $\tilde{\rho}^{(n)} = FT[\rho^{(n)}]$;

(b) $\mathbf{E}^{(n)} = \mathbf{E}^{ex} - \frac{i}{\varepsilon_0} FT^{-1}[\frac{\tilde{\rho}^{(n)}}{k}\mathbf{n}]$;

(c) $\tilde{\rho}_{tb}{}^{(n)} = -i\mathbf{k} \cdot FT[\varepsilon_0 \chi \mathbf{E}^{(n)}]$, $\rho_{tb}{}^{(n)} = FT^{-1}[\tilde{\rho}_{tb}{}^{(n)}]$;

(d) Update ρ_b by $\rho_b{}^{(n+1)} = \rho_b{}^{(n)} + \Delta\rho_b{}^{(n)}$ with $\Delta\rho_b{}^{(n)} = \lambda[\rho_{tb}{}^{(n)} - \rho_b{}^{(n)}]$, and repeat Operations (a-d) unless when $\max(\left|\rho_{tb}{}^{(n)} - \rho_b{}^{(n)}\right|) < \delta_\rho$ is achieved (convergence criterion).

In the above formula δ_ρ is a predefined small number for controlling the target precision, and λ is a coefficient, generally chosen to be $\sim 1/\bar{\varepsilon}_r$, where $\bar{\varepsilon}_r$ is the maximum permittivity in the model or permittivity contrast if the minimum ε_r in the system is 1 (The determination of λ will be discussed later). Operation (b) is to calculate the electric field by the assumed charge density at the *n*th step according to Eq. (5). If completely unknown, the initial value of bound charge density can be set as

$$\rho_b{}^{(0)}(\mathbf{r}) = -\rho_f(\mathbf{r})\chi(\mathbf{r})/[1+\chi(\mathbf{r})] \ . \tag{0}$$

In Operation (b) the electric field satisfies Gauss's law of

$$\nabla \cdot \mathbf{E}^{(n)}(\mathbf{r}) = [\rho_b{}^{(n)}(\mathbf{r}) + \rho_f(\mathbf{r})]/\varepsilon_0 . \tag{0}$$

Operation (c) is to tentatively evaluate the bound charge according to the constitutive equation, $\rho_{tb}{}^{(n)} = -\nabla \cdot [\varepsilon_0 \chi \mathbf{E}^{(n)}]$, by the spectral method. Operation (d) means to minimize the difference between $\rho_{tb}{}^{(n)}$ and the assumed bound charge, $\rho_b{}^{(n)}$, because if $\rho_{tb}{}^{(n)} = \rho_b{}^{(n)}$ is achieved, by Eq. (8) one obtains $-\nabla \cdot [\varepsilon_0 \chi \mathbf{E}^{(n)}] = \varepsilon_0 \nabla \cdot \mathbf{E}^{(n)} - \rho_f$ which leads to

$$\nabla \cdot [\varepsilon_r(\mathbf{r})\varepsilon_0 \mathbf{E}^{(n)}(\mathbf{r})] = \rho_f(\mathbf{r}) . \tag{0}$$

In other words, given any initial input of $\rho_b{}^{(0)}$, as long as the bound charge density calculated from the constitutive law agrees with its assumed value, the solved electric field satisfies the general form of Gauss's law within a given accuracy.

Now we need to determine the coefficient λ. Combination of the constitutive equation in Operation (c) and Eq. (8) yields

$$\rho_{tb}^{(n)}(\mathbf{r}) - \rho_b^{(n)}(\mathbf{r}) = -\varepsilon_0 \nabla\chi(\mathbf{r}) \cdot \mathbf{E}^{(n)}(\mathbf{r}) - \chi(\mathbf{r})\rho_f(\mathbf{r}) - [1+\chi(\mathbf{r})]\rho_b^{(n)}(\mathbf{r}) \tag{0}$$

From Eq. (6), the difference between the true solution ρ_b and $\rho_b^{(n)}$ is

$$\rho_b(\mathbf{r}) - \rho_b^{(n)}(\mathbf{r}) = \frac{-\varepsilon_0}{1+\chi(\mathbf{r})} \nabla\chi(\mathbf{r}) \cdot \mathbf{E}(\mathbf{r}) - \frac{\chi(\mathbf{r})}{1+\chi(\mathbf{r})} \rho_f(\mathbf{r}) - \rho_b^{(n)}(\mathbf{r}) \tag{0}$$

Comparing Eqs. (10) and (11), and by assuming $\nabla\chi \cdot \mathbf{E}^{(n)}$ is on the same order of $\nabla\chi \cdot \mathbf{E}$,[†] one finds that $\rho_b - \rho_b^{(n)} \sim (\rho_{tb}^{(n)} - \rho_b^{(n)})/(1+\chi)$. For this sake, we choose $\lambda \sim 1/\bar{\varepsilon}_r$. As the value of $1+\chi$ may be spatially varying from 1 to $\bar{\varepsilon}_r$, choosing $\lambda = 1/\bar{\varepsilon}_r$ would allow the bound charge to be retrieved by a fraction of $\sim 1/\bar{\varepsilon}_r$ or above at any position. Subsequently, the maximum error of bound charge density at the *n*th step

$$\Delta^{(n)} = \max\left(\left|\rho_b(\mathbf{r}) - \rho_b^{(n)}(\mathbf{r})\right|\right), \tag{0}$$

is expected to be roughly a geometric series with a common ratio of $1 - 1/\bar{\varepsilon}_r$. From this inference the number of iterations required (*I*) to reach a target precision δ_ρ^* (normalized by the maximum bound charge density in the model) is expected to be on the order of

$$I = \frac{\ln \delta_\rho^*}{\ln(1 - 1/\bar{\varepsilon}_r)}. \tag{0}$$

This estimation is based on the assumption that the initial error of bound charge is ~100%, and the iteration number could be even less if the initial input $\rho_b^{(0)}$ is already close to the final solution ρ_b (instead of simply using Eq. (7)). It appears unlikely to have such input of $\rho_b^{(0)}$ but later we will show how it is feasible in diffuse-interface models.

Rigorously proving the convergence of BCSA in a general situation is probably difficult (see the Appendix for more discussions). Whereas, our extensive numerical tests show that this algorithm

[†] Close to convergence this assumption must be true. At the beginning steps, if the input of bound charge density is far from the solution, in principle $\nabla\chi \cdot \mathbf{E}^{(n)}$ may not necessarily be on the same order of $\nabla\chi \cdot \mathbf{E}$. However, all our numerical tests show that as long as λ is small enough ($\lambda \sim 1/\bar{\varepsilon}_r$), convergence can always be reached in limited steps estimated by Eq. (13), even with a poor initial guess, such as by using Eq. (7).

is very robust and that Eq. (13) does provide a good estimate for the number of steps required for simple as well as very complex systems.

III. Simulation results: verifications and applications of the BCSA algorithm

A. Verification on the validity/accuracy

To check the validity of the BCSA algorithm, calculating the depolarization factor (DF) of an ellipsoid is first considered. Assume the ellipsoid is placed in vacuum and it has homogeneous dielectric susceptibility χ subject to a uniform external electric field $\mathbf{E}^{ex}$ along one of its principal axes. The actual macroscopic electric field inside the ellipsoid is also uniform according to the strict analytical solution (based on the sharp interface model) [1], given by

$$\mathbf{E} = \frac{\mathbf{E}^{ex}}{1 + N\chi} , \tag{0}$$

where N is the DF for the principal axis. For an arbitrary ellipsoid N is positive and generally less than 1 with the sum of N's for all three principal axes equal to 1 [38]. To compare the calculated DFs with the analytical solution, we need the diffuse interface model to approach the sharp interface limit, i.e., $t << \Delta$, where t is the characteristic interface thickness and Δ the characteristic size of the material structure. In addition, in this case the effect of periodic boundary condition must be minimized, which requires $\Delta << L$ where L the computational domain size. ε_r is set as 10 inside the inclusion and it smoothly transits across the surface to 1 outside. A two-dimensional mesh of 1024×1024 is used and the major axis of the ellipse is discretized into 60~100 grid points (depending on the aspect ratio of ellipses). This simulation corresponds to an infinitely long cylinder with an elliptical cross-section thus N in the length direction is zero. δ_ρ^* is set to 0.001. Figure 2 shows the numerical solution of electric field and bound charge distribution of a special case, a circular particle, where positive and negative bound charge is developed at the upper and lower parts of the surface, respectively.

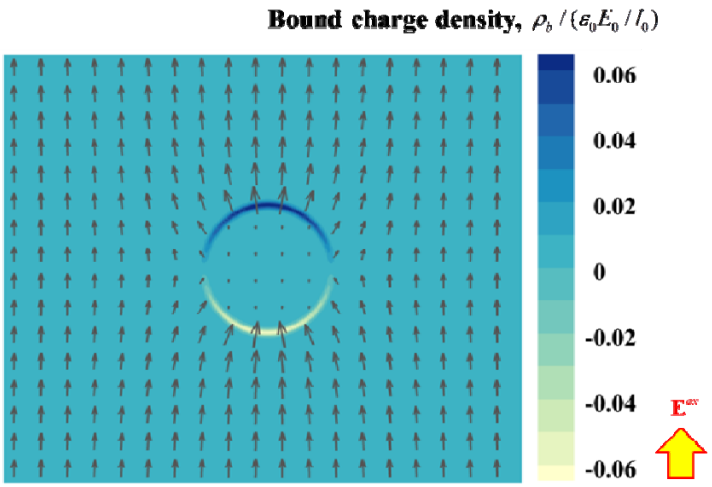

FIG. 2. (Color online) Calculated bound charge density distribution as a circular dielectric inclusion is placed in a uniform external electric field ($|\mathbf{E}^{ex}|=0.1E_0$), the length and direction of the arrows represent the magnitude and direction of the local electric field.

It is noted that the coefficient $\lambda=1/\bar{\varepsilon}_r$ works for all tested cases but other value could be used too. For all tested configurations (all the simulation cases in this paper) the algorithm fails to converge with $\lambda\geq 2/\bar{\varepsilon}_r$ and the optimal value λ (λ_O) is found to fall between $1/\bar{\varepsilon}_r$ and $2/\bar{\varepsilon}_r$ for different systems. The value of $2/\bar{\varepsilon}_r$ appears to be a threshold value beyond which strong oscillation and divergence occur. For the simulation in Fig. 2, when $\lambda=1/\bar{\varepsilon}_r$ BCSA requires 48 iterations to converge, while the least iteration number is 26 by using $\lambda_O=1.7/\bar{\varepsilon}_r$. This suggests that in the future λ could be further optimized dynamically to achieve the best efficiency.

Mejdoubi and Brosseau (MB) solved the same DF problem for ellipses of different aspect ratios by combining a series expansion of Maxwell-Garnett and Bruggeman models and finite element analysis (FEA) [16]. On the other hand, an analytical solution exists for the infinite elliptical cylinder situation that is simply $N=a/(a+b)$ where a and b denote the semi-major and semi-minor axes of the ellipse, respectively [38]. The results of MB with second order approximation and the exact solution together with our simulation results are shown for comparison (Fig. 3 and Table 1). It is shown that the simulation results, based on the diffuse-interface approach, have surprisingly good accuracy for the calculation of DFs as the simulation model is approaching the

sharp interface limit. The accuracy is even better than the FEA based results of MB for some large aspect ratio cases.

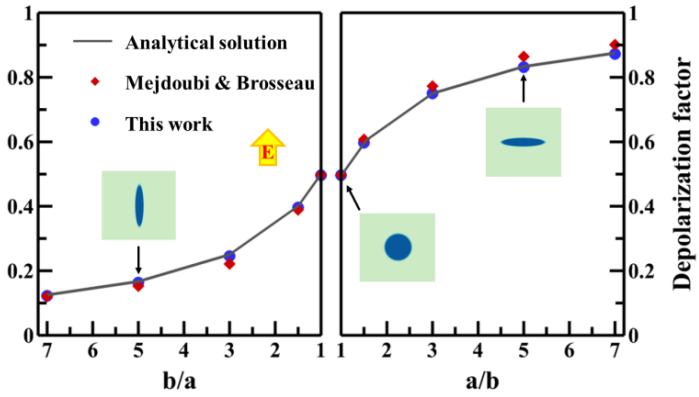

FIG. 3. (Color online) Calculated depolarization factors for ellipses of different aspect ratios as compared with the results by Mejdoubi and Brosseau [16], and the analytical solution of Osborn [38].

Table 1. Depolarization factors calculated in this work as compared with analytical solution and the simulation results of Mejdoubi and Brosseau (MB) [16].

	a/b=7	a/b=5	a/b=3	a/b= 3/2	a/b=1 (disk)	b/a= 3/2	b/a=3	b/a=5	b/a=7
This work	0.872	0.831	0.750	0.597	0.496	0.396	0.245	0.163	0.122
MB results	0.901	0.864	0.772	0.607	0.497	0.389	0.221	0.152	0.120
Analytical solution	0.875	0.833	0.750	0.600	0.500	0.400	0.250	0.167	0.125

B. Simulation of complex dielectric heterostructure and performance study of the BCSA algorithm

For a given numerical grid, the computational cost of the BCSA algorithm only depends on the permittivity contrast of the model as estimated by Eq. (13), almost independent of the geometry or topology of the structure. This feature is manifested by a demonstrative simulation where the system consists of various arbitrarily selected inclusions in a medium, including polygons,

concave/convex profiles, hollow, nested and core-shell structures with local relative permittivity distribution shown in Fig. 4a (readers are referred to Refs. [16, 39] for related studies on the electrostatics regarding some of these geometries). This case probably represents an extreme case of random composite materials. Before running the simulation the created geometries are numerically 'polished' so that the susceptibility smoothly transits across all the interfaces. Figure 4b shows part of the simulation result where the color denotes the vertical component of electric field and the direction and length of arrows represent the direction and magnitude of local electric field (yet macroscopic), with a uniform external field $\mathbf{E}^{ex}$ applied in the vertical direction (y-axis). The spots of electric field concentration imply possible locations of dielectric breakdown. The polarization density field can be obtained via Eq. (4) as the electric field is solved. Similarly, one may apply the external field in the x direction and calculate the polarization density again. The effective permittivity tensor of this 'composite' can then be evaluated following the strategy outlined in Ref. [29]. More detailed analysis on this structure is beyond the scope of this paper, as the purpose here is to demonstrate the capability and efficiency of the numerical algorithm.

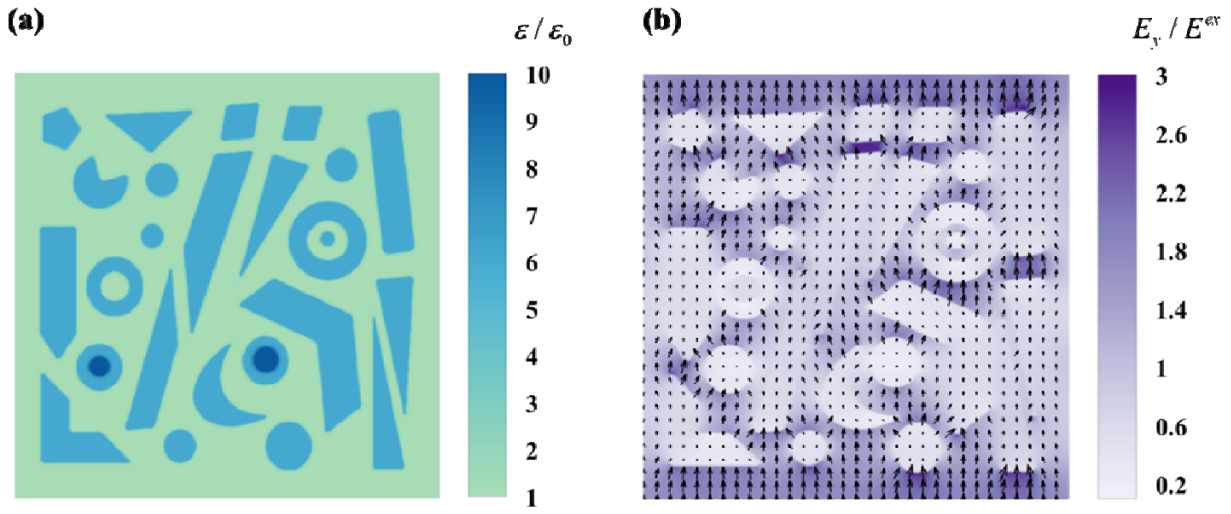

FIG. 4. (Color online) Solution of electrostatics in a random dielectric heterostructure subject to a uniform external electric field. (a) distribution of local relative permittivity; (b) distribution of the y-component of electric field, normalized by the magnitude of external electric field. The direction and length of arrows indicate the direction and magnitude of local electric field.

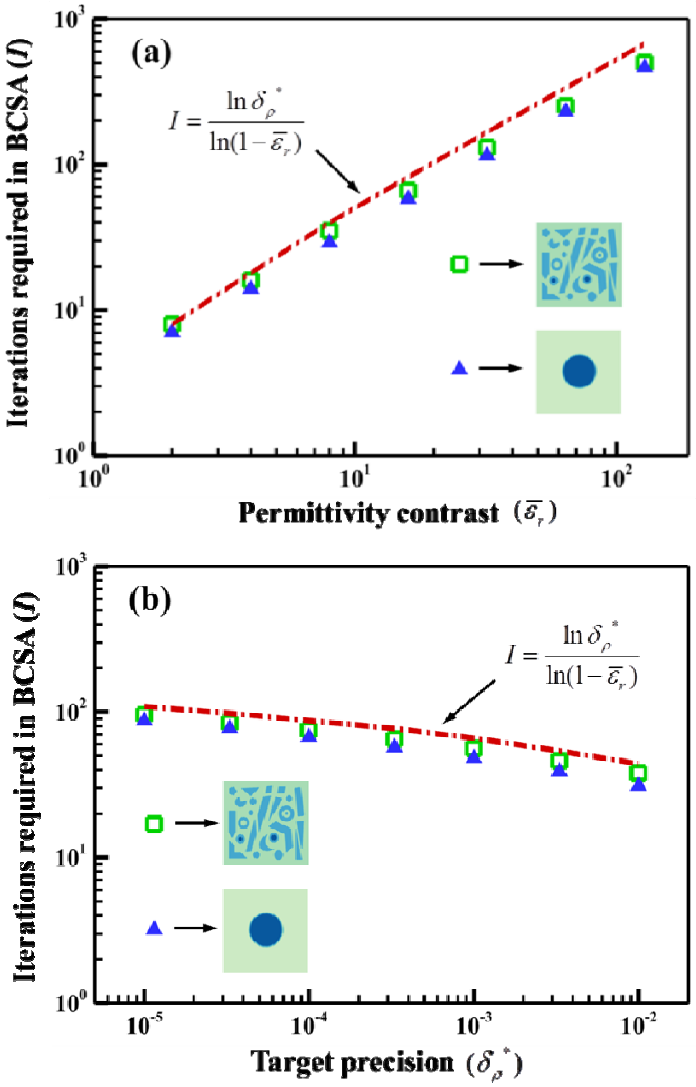

FIG. 5. (Color online) Study on the performance of the BCSA algorithm. (a) simulations with different permittivity contrast; (b) simulation with different target precision.

To quantitatively check the performance of the BCSA algorithm and its adaptability to structures with different degree of complexity, we perform two parametric studies. In the first one, the permittivity contrast ($\bar{\varepsilon}_r$) of the models is rescaled from 2 to 128. In the second one, the target bound charge precision (δ_ρ^*) varies from 10^{-2} down to 10^{-5}. For comparison, we use two different structures for the two parametric studies, respectively. One is the simple sphere as shown in Fig.2, and the other is the complex structure as shown in Fig. 4 (the numerical grids used are both 1024×1024). The results are shown in Fig. 5. Surprisingly and interestingly, the

iteration number required in BCSA for the complex structure is only a little more than that for the simple structure for all the tested δ_ρ^* and $\bar{\varepsilon}_r$ combinations, and for all the cases the iterations required are well estimated by Eq. (13). Actually, Eq. (13) apparently represents an upper limit for the required iterations (steps) in BCSA. These results demonstrate that the maximum error of bound charge density indeed decreases approximately following a geometric series, thus the algorithm is programmed to converge in limited steps, which is a unique feature of this algorithm. The above results also indicate that with the same numerical grids and same permittivity contrast, the computational cost of BCSA for solving electrostatics in a complex structure like in Fig. 4 is virtually the same as a simple structure as in Fig. 2. The computational cost of sharp interface based numerical methods usually relies on the complexity of structure (cf. e.g., [18, 20, 26, 28]). Therefore, the diffuse-interface based BCSA algorithm may have increased advantage in numerical efficiency as compared to the sharp interface based approaches with increasing complexity of the heterostructure. Of particular note, a time-dependent Ginzburg-Landau (TDGL) type equation has been employed to minimize the free energy functional so as to equivalently solve the general Gauss's law (Eq. (1)) in Wang's algorithm [29]. This algorithm is also based on the diffuse-interface approach. Nevertheless, the BCSA algorithm apparently has advantage in terms of computational efficiency as compared to the TDGL-based algorithm. We also find it possible to optimize the kinetic coefficients in the TDGL equation to reduce the difference between the two algorithms in efficiency (see the Appendix for more detailed discussion).

C. Simulation of an evolving heterostructure: the RLTI scheme

In time-dependent problems the electrostatics needs to be reevaluated in each time step as long as either the permittivity field $\varepsilon(\mathbf{r})$ or the free charge density $\rho_f(\mathbf{r})$ is changed, even slightly. If one directly solves Poisson's equation (e.g., modeling of the electrodeposition process [40]), each time step would be equally expensive in computational cost. However, when there are only slight changes in $\varepsilon(\mathbf{r})$ and/or $\rho_f(\mathbf{r})$ in a time step, the bound charge distribution is expected to change also slightly. Provided this is true, in the BCSA algorithm the bound charge solution in one time step could be used as an input for the next, which we call a RLTI scheme (Result of Last Time step as Input). We show that such a scheme could significantly shorten the approximation (iteration) process.

In the following example, the RLTI scheme is applied to simulation of an evolving heterostructure caused by motion of a group of colloidal particles, a typical process in dielectrophoresis or magnetophoresis. The electrostatic interaction is fully accounted, instead of using the simplified DEP force formula that is based on the assumption of an isolated small spherical particle [4]. The initial set-up is shown in the first panel of Fig. 6 where twenty one particles are placed in a random fashion. A nonuniform external field is generated by two oppositely charged poles (fixed in this work) next to these particles. The particles are thus expected to undergo DEP forces. However, for the multiple-particle problem there is also complex electrostatic interaction among the particles. In our simulation each particle is modeled by a template field variable subject to rigid body translation and rotation (by interpolation to the fixed background grid) under external force/torque, the so-called diffuse-interface field approach (DIFA), first proposed by Wang [41].

Each particle α is described by a template field variable $\eta_\alpha(\mathbf{r})$ whose value is 1 inside the particle and 0 outside. The particle interfaces possess approximately $3l_0$ thickness between 10% and 90% of η values (in the surface normal direction the profile of $\eta_\alpha(\mathbf{r})$ is similar to the susceptibility profile shown in Fig. 1b). The particle radius is approximately $10l_0$, where l_0 is the unit grid size. Each particle is attached with a 'halo' field $\tilde{\eta}_\alpha(\mathbf{r})$ [42] which has a similar profile of $\eta_\alpha(\mathbf{r})$ except that the radius of particle halo is set to be slightly larger than the particle core, approximately $14l_0$ in this work. This 'halo' field is introduced for convenience of defining more detailed particle structure and for better numerical accuracy in resolving interparticle forces between close particles [42]. Here the short range interparticle repulsions are defined based on the halo fields to avoid particle overlapping by $\mathbf{F}^{\mathrm{sr}}(\alpha) = \int \kappa \sum_{\alpha \neq \alpha'} \tilde{\eta}_\alpha(\mathbf{r})\tilde{\eta}_{\alpha'}(\mathbf{r})[\nabla\tilde{\eta}_\alpha(\mathbf{r}) - \nabla\tilde{\eta}_{\alpha'}(\mathbf{r})]\mathrm{d}^3\mathrm{r}$, where κ is a penalty coefficient [41]. The two poles are just modeled by two bigger particles carrying free charge density defined as $\rho_f(\mathbf{r}) = \sum_{\beta=1,2} \rho_\beta{}^0 \eta_\beta(\mathbf{r})[1-\eta_\beta(\mathbf{r})]$ [35] with $\rho_1{}^0 = -\rho_2{}^0 = \rho^0$. The dielectric constant is defined as $\varepsilon(\mathbf{r}) = 7\varepsilon_0 \sum_{\alpha=1,21} \eta_\alpha(\mathbf{r}) + \varepsilon_0$, which means ε

in the bulk particle is eight times of that in the carrier liquid. The $\varepsilon(\mathbf{r})$ profile changes with the movement of particles. Assume there is only bound charge on the particles, each particle α undergoes total electrostatic force of $\mathbf{F}^{\mathrm{el}}(\alpha)=\int \rho_{\mathrm{b}}(\mathbf{r})\tilde{\eta}_{\alpha}(\mathbf{r})\mathbf{E}(\mathbf{r})\mathrm{d}^3\mathrm{r}$.

The carrier liquid is assumed to be viscous so the Reynolds number is low and the particles move only in the presence of external force/torque. The relationship between particle motions and external forces is linked by mobility matrix, derived by isolated particle in unbounded fluid [41, 43], and hydrodynamic interaction between particles is not considered. For the sake of simplicity, gravity, Brownian forces, van der Waals forces, and particle rotations are all neglected in this work. The external forces each particle α undergoes include electrostatic force $\mathbf{F}^{el}(\alpha)$ and short-range repulsion $\mathbf{F}^{sr}(\alpha)$ when the particle is in contact with another one (or the poles). The external force, $\mathbf{F}^{ex}(\alpha)=\mathbf{F}^{sr}(\alpha)+\mathbf{F}^{el}(\alpha)$, is balanced by the Stokes drag force and the particle velocity is linked to external force by $\mathbf{U}(\alpha)=\mathbf{M}(\alpha)\mathbf{F}^{ex}(\alpha)$. The mobility coefficient is set as $M_{ij}(\alpha)=M_0\delta_{ij}$, where δ_{ij} is Kronecker delta (for a sphere $M_0=1/6\pi\mu a$, where a the particle radius and μ the dynamic viscosity of the carrier liquid). The simulation time step is set as $t_0=\varepsilon_0/(M_0\rho_0^2 l_0^3)$.

As shown in Fig. 6, the nearest particles are attracted to move toward the positively charged pole due to the electric field gradient. Fig. 7a shows the real-time local electric field in the dashed box of Fig. 6 (at time step of 6,000), compared with Fig. 7b that is the distribution of external electric field generated by the poles in the same zone. The local electric field is seriously altered due to the presence of particles thus the isolated-particle assumption (in the simplified DEP force formula) is invalid. In this simulation, δ_{ρ}^{*} is set to 0.005 and $\lambda=1.7/\bar{\varepsilon}_r=0.17$ is used. In the first time step, the input of bound charge is set by Eq. (7), which leads to $\rho_b^{(0)}(\mathbf{r})=0$, and in that time step the BCSA algorithm requires 16 iterations . However, with the RLTI scheme being applied to all subsequent time steps, the average iteration number per time step in the entire simulation is reduced to only about 3.2 (Fig. 8).

Figure 8 further shows the relationship between the iterations required in BCSA algorithm and maximum particle displacement with time during the simulation. When particle displacement is small, the bound charge distribution has limited change within one time step, and as a result, the BCSA algorithm requires only a few iterations. This situation is maintained until one particle is attracted to be very close to one of the poles when the strong electrostatic force causes quick particle movement (Time Step=9000 in Fig. 6). Subsequently, the solution of bound charge density in the previous time step becomes a poor initial input due to the large particle displacement (per time step). When the particle is finally attached to the pole (the last panel in Fig. 6) the strong electrostatic force is balanced by the short-range repulsion between the particle and the pole, leading to smaller maximum particle displacement. Thus, except for the short period when the particle is approaching the pole, the maximum particle displacement is small and the RLTI scheme is very effective. As is shown in Fig. 8, as long as the maximum particle movement (or say, maximum shift of the interface) is less than ~0.1 grid size in a time step, the iterations required can be significantly reduced by using the RLTI scheme. For the sake of numerical reliability and stability, during time discretization of the governing differential equations the time step is usually small in diffuse-interface models especially when an explicit scheme is employed [32], and as a result, the maximum shift of interface in a time step is commonly small. The RLTI scheme is expected to be applicable to many diffuse-interface (phase-field) models for microstructural evolution modeling also in considerations that: (a) most diffuse-interface models are coarsen-grained or continuum models, and in bulk regions (away from the interfaces) the spatially distributed field variables usually change mildly within a time step; (b) at the interfaces the field variables transit continuously and smoothly therefore even when an interface is moving the values of field variables usually do not jump at the interfaces, in contrast to sharp interface models.

Note that the main purpose here is to demonstrate the performance of the BCSA algorithm in calculating the electrostatic interactions in an evolving structure. For realistic simulation of dielectrophoresis processes, even in small Reynolds number regime the long range hydrodynamic interaction between particles needs to be incorporated [43, 44]. We have performed some preliminary study to introduce the long range hydrodynamic interaction through the Green's function (Stokeslet) [45], following the method proposed by Kirkwood and Riseman

[46]. Our preliminary results show that the Stokeslet interaction does affect particle motion appreciably, while the RLTI scheme and BCSA algorithm still work efficiently (with the same time step the average iteration numbers in BCSA is slightly larger since the maximum particle displacement is generally increased with the Stokeslet interaction included). This is expected as the effectiveness of the RLTI scheme only depends on the particle (interfacial) displacement in each time step, irrespective of the forces that govern particle motion. Further development of the model is ongoing and the results would be published elsewhere. It is also possible to introduce other numerical methods to directly solve hydrodynamics in our future work, and the Lattice Boltzmann method is possibly a good candidate [47] .

Modeling electrophoresis or dielectrophoresis of multiple particles is a typical case of evolving dielectric heterostructure that requires real-time solution of the electrostatics. The related material process could be used as an effective approach to fabrication of functional composites with engineered microstructure under external field control (the colloidal assembly would be used as a precursor to fabrication of composites). Another example of evolving heterostructure is, the growth of oxide film on metal surface during high temperature metal oxidation, which has been explored in our previous modeling work [48, 49] where the BCSA algorithm and the RLTI scheme have already been used. In that oxidation model the gas-oxide-metal phases are treated as a dielectric heterostructure. Both the dielectric structure and the free charge distribution (caused by charged point defects) evolve during the growth of oxide film. However, the growth of the oxide film is a sluggish process, and as a result with the RLTI scheme the average iteration number needed per time step in the BCSA algorithm is only slightly more than 1. Thus, the BCSA algorithm allows the real-time calculation of electrostatic interaction to be very efficient in the model.

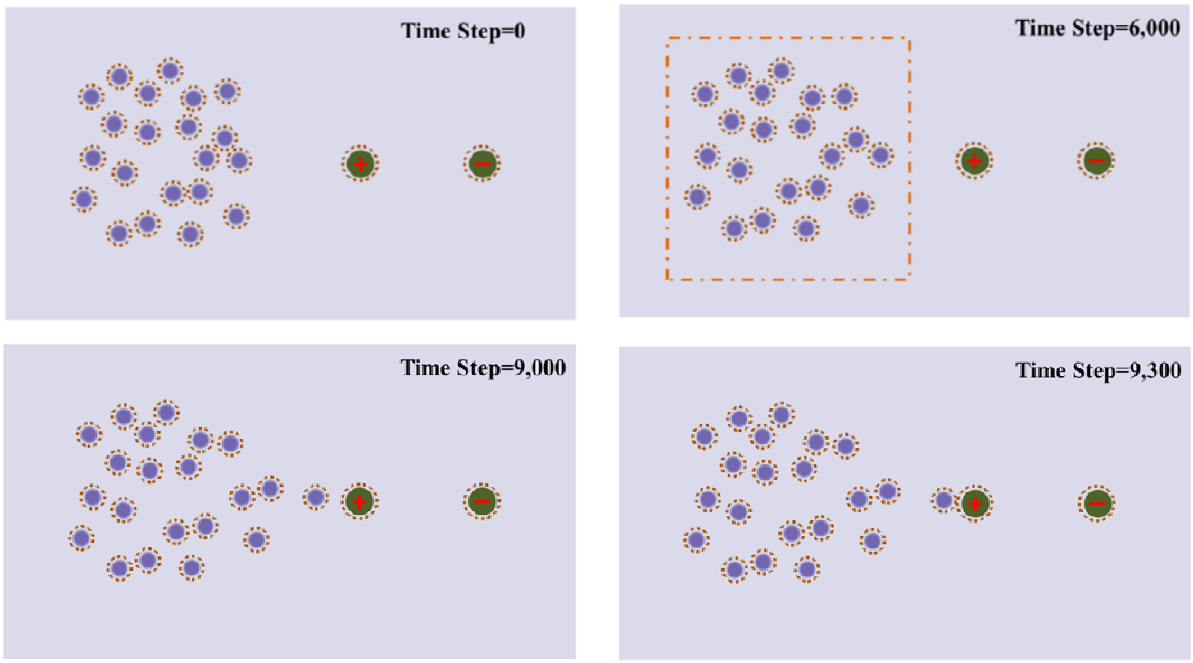

FIG. 6. (Color online) Simulation of colloidal particles movement under electrostatic forces by using diffuse-interface field approach (DIFA) and the BCSA algorithm. Randomly distributed circular particles are attracted by two fixed oppositely charged poles. The dashed line around each particle indicates the 'halo' of that particle. The signs of charge on the poles are manually added for visual aid.

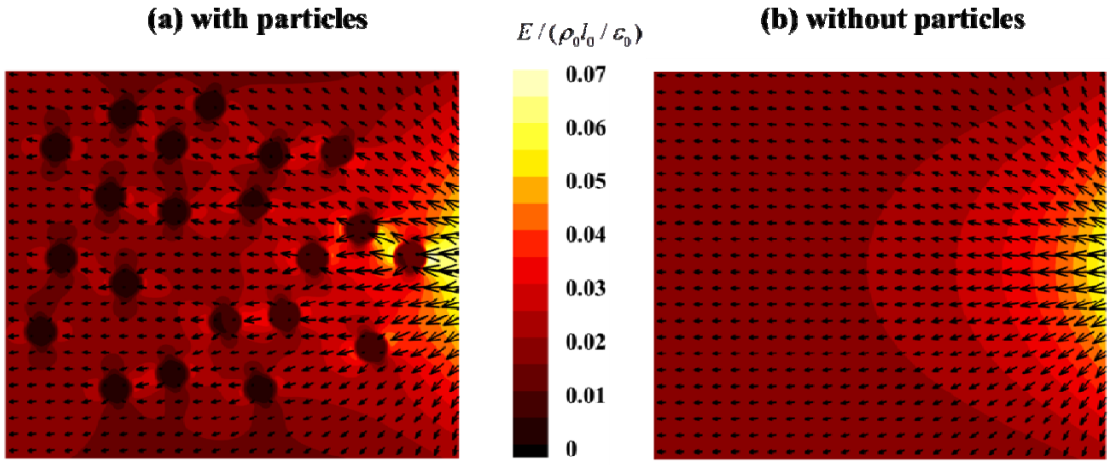

FIG. 7. (Color online) (a) Electric field distribution inside the dash-dot box in Fig. 6. The color represents the local magnitude of electric field (normalized by $\rho_0 l_0 / \varepsilon_0$) and the arrows indicate

the local direction. (b) External electric field in the same zone as (a), calculated by removing the particles.

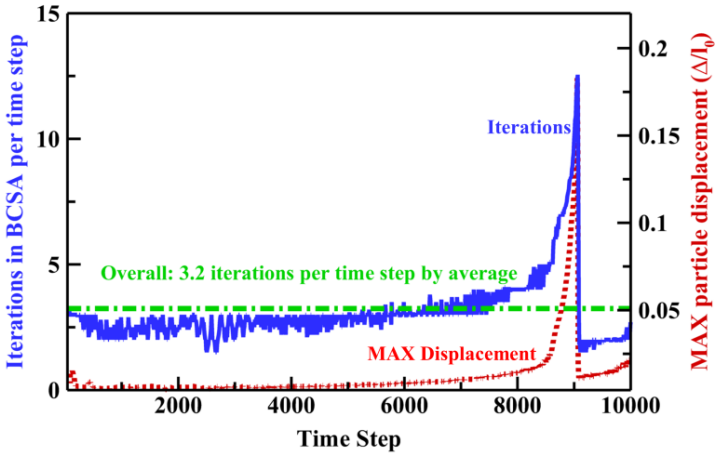

FIG. 8. (Color online) The real-time iterations needed (averaged per 10 time steps) in the BCSA algorithm corresponding to Fig. 6 (solid blue line), with the red dot line denotes the maximum particle displacement in a time step during evolution. By applying the RLTI scheme the overall mean required iterations in BCSA is only 3.2 (dashed green line).

IV. Magnetostatics involving a heterostructure

The proposed BCSA algorithm has shown to be very efficient to solve complex and evolving electrostatic heterogeneity problems. Magnetostatic problems involving spatially varying magnetic susceptibility can be solved following the same methodology by virtue of the mathematical analogy (cf. [29]). The governing equation for magnetostatic problems is (Gauss's law for magnetism)

$$\nabla \cdot \mathbf{B}(\mathbf{r}) = \nabla \cdot [\mu_0 (1 + \chi(\mathbf{r}))\mathbf{H}(\mathbf{r})] = 0\,, \tag{0}$$

where $\mathbf{H}(\mathbf{r})$ is the magnetic field strength, $\mathbf{B}(\mathbf{r})$ the magnetic induction, μ_0 free space permeability, and $\chi(\mathbf{r})$ the (magnetic) susceptibility (linear susceptibility is also assumed). Equation (15) is parallel to Eq. (1) except that free magnetic charge (magnetic monopole) has never been found in nature. The magnetic charge analogous to the bound charge in dielectrics is

$$\rho_m = -\nabla \cdot \mathbf{J}(\mathbf{r}) = -\nabla \cdot [\mu_0 \chi(\mathbf{r})\mathbf{H}(\mathbf{r})], \tag{0}$$

where $\mathbf{J}(\mathbf{r})$ is the magnetic polarization density. The mathematical analogy is apparent and a version of BCSA algorithm for magnetostatics is given in Algorithm 2 for convenience. The initial input $\rho_m^{(0)}$ can be set as zero or by using the RLTI scheme for an evolving structure. The coefficient λ needs to be set to $\sim 1/\bar{\mu}_r$, where $\bar{\mu}_r$ is the permeability contrast in the system (the optimal λ is typically between $1/\bar{\mu}_r$ and $2/\bar{\mu}_r$). Actually, the concept of magnetic charge has been frequently used in the literature to help analyze magnetostatic interactions (e.g., [50-52]). However, it appears an efficient numerical algorithm that directly solves the magnetic charge density as the primary field variable has not been reported so far.

Algorithm 2: BCSA algorithm for magnetostatics

(a) $\tilde{\rho}_m^{(n)} = FT[\rho_m^{(n)}]$;

(b) $\mathbf{H}^{(n)} = \mathbf{H}^{ex} - \frac{i}{\mu_0} FT^{-1}[\frac{\tilde{\rho}_m^{(n)}}{k}\mathbf{n}]$

(c) $\tilde{\rho}_{tm}^{(n)} = -i\mathbf{k} \cdot FT[\mu_0 \chi \mathbf{H}^{(n)}]$, $\rho_{tm}^{(n)} = FT^{-1}[\tilde{\rho}_{tm}^{(n)}]$;

(d) Update ρ_m by $\rho_m^{(n+1)} = \rho_m^{(n)} + \Delta\rho_m^{(n)}$ with $\Delta\rho_m^{(n)} = \lambda[\rho_{tm}^{(n)} - \rho_m^{(n)}]$, and repeat Operations (a-d) unless when $\max(\left|\rho_{tm}^{(n)} - \rho_m^{(n)}\right|) < \delta_\rho$ is achieved (convergence criterion).

Comparing Algorithms 2 and 1, one finds that with appropriate normalization the previous results regarding dielectric heterogeneity can be immediately translated into solutions for the corresponding magnetic heterogeneity problems (cf. [16]). For example, one may normalize the charge density by $\varepsilon_0 E_0 / l_0$ (E_0 and l_0 are the units for electric field and length), and then Eq. (1) after nondimensionalization is $\nabla^* \cdot [(1+\chi)\mathbf{E}^*] = \rho_f^*$. This equation is numerically equivalent to $\nabla^* \cdot [(1+\chi)\mathbf{H}^*] = \rho_m^*$ (the dimensionless dielectric susceptibility just corresponds to the magnetic susceptibility). As long as one replaces the unit electric field strength E_0 with the unit magnetic field strength H_0 (the magnetic bound charge density unit is accordingly $\mu_0 H_0 / l_0$), the previously calculated electric field and bound charge can be alternatively interpreted as magnetic field and magnetic bound charge. Subsequently, the simulation results in Fig. 3 and Fig. 4 can

also be interpreted as calculations for the demagnetization factors of ellipsoids [38], and magnetic mixtures (composites), respectively. For the dielectrophoresis problem in Fig. 6, one might need to additionally replace the two charged poles with a permanent magnetic dipole to induce correspondingly the magnetophoresis phenomenon, since free charge is meaningless in magnetics.

V. Discussions

In some variational approaches vector function variables (polarization and magnetic polarization) are frequently involved and subsequently Ginzburg-Landau type equations (e.g., [29]) or Landau-Lifshitz-Gilbert equations (e.g., [50]) are used to minimize the free energy functional. Such processes are often computationally costly, partly due to the small time step requirement (see the Appendix for more detailed discussions). The BCSA algorithm solves the scalar bound charge density thus the degree of freedom of the system is reduced, and by our verification the algorithm only requires limited iteration number estimated by Eq. (13). Note that if the minimum permittivity of the system, ε_{rm}, is larger than one then $\varepsilon_r(\mathbf{r})$ can be normalized by ε_{rm}, which only requires to normalize $\rho_f(\mathbf{r})$ simultaneously by a factor of ε_{rm} in Algorithm 1. If the dielectric contrast is close to unity ($\bar{\varepsilon}_r \to 1$, or $\chi \to 0$) in the model, the iteration number (I) goes to nearly zero by Eq. (13), which is not surprising because in that case the electric field calculated from Eq. (5) is just the solution. The same situation is in Algorithm 2. Therefore, only the permittivity/permeability contrast matters.

It is worth discussing the choice of parameter δ_ρ^* (the target precision). Fig. 5 has demonstrated the convergence behavior of the BCSA algorithm. The error of bound charge density approximately diminishes following a geometric series, and by Eq. (13) if one decreases the target precision by one order of magnitude, the extra iterations required is just on the order of $\Delta I = \ln 0.1 / \ln(1 - 1/\bar{\varepsilon}_r)$. However, the numerical precision just measures the difference between the result and the best achievable result (with sufficient iterations) by this algorithm, and depending on the specific problem this precision is not equivalent to the actual accuracy of the model. For example, in calculating the depolarization factors (see Fig. 3 & Table 1), the slight

mismatch between the simulation result and the analytical solution cannot be eliminated simply by reducing δ_ρ^* to infinitesimal. This is due to that there could be systematic error caused by other factors, such as whether t/Δ is sufficiently small (requirement for approaching the sharp interface limit). On the other hand, while analytical solutions based on sharp-interface description are often used for verification purpose, for a real material problem a sharp-interface model itself is an approximation. Even with analytical solution available, it does not necessarily represent more accurate result, for the real material interface always has finite thickness and is diffuse in nature.

In the BCSA algorithm, the iteration steps can be further reduced if the input of bound charge density is already close to the final solution. Subsequently, the simple RLTI scheme is found to be very effective in simulations of evolving structures via the diffuse-interface approach. In contrast, for sharp interface models due to the interfacial discontinuity it is difficult to apply the RLTI scheme to the moving interface regimes. Guyer *et al* developed an elegant diffuse-interface (phase-field) model for the electrodeposition/electrodissociation processes [40, 53]. In their kinetic model Poisson's equation was solved in every time step, which was a bottleneck for applying the model to higher dimensional cases [40]. This issue could be resolved by using the BCSA algorithm together with the RLTI scheme. The governing kinetic equation only requires to solve $\nabla\phi$ which is equal to $-\mathbf{E}$, although with the electric field solved the electrostatic potential can be conveniently obtained by integration. The computational cost for each iteration in BCSA is mainly determined by the FFT operations, while it is well known that the time complexity of FFT is only $O(M \ln M)$, where M is the total number of the discrete grid points in the model. When only several times of FFT operations are required in each time step (on average), directly solving electrostatics in a complex and evolving heterostructure becomes affordable for common computers nowadays.

VI. Conclusion

The simple and easy-to-implement BCSA algorithm developed in this work shows to be very efficient in solving electrostatic/magnetostatic heterogeneity problems. Formulated in the context of diffuse-interface (phase-field) modeling, this algorithm is general to accommodate

heterogeneity of the permittivity/permeability and the free charge density. By our analysis and numerical tests, during the approximation process the error of bound charge density diminishes approximately following a geometric series with a common ratio of $1-1/\bar{\varepsilon}_r$ with $\bar{\varepsilon}_r$ being the permittivity/permeability contrast in the whole system. The time complexity of this algorithm is thus nearly independent of the complexity of the geometry. In particular, for simulation of an evolving heterostructure the RLTI scheme could further significantly reduce the computational cost as the spatially varying field variables smoothly evolve from one time step to the next. We believe the proposed algorithm here combined with the diffuse-interface approach opens a promising route to simulate complex and/or evolving dielectric/magnetic heterostructures.

Appendix: On the convergence of the BCSA algorithm

The BCSA algorithm shows impressive convergence performance even without using the RLTI scheme. This algorithm, however, is not derived from the functional minimization method such as in Wang's phase-field model for composites [29]. Both Wang's method and our algorithm are based on the framework of diffuse-interface modeling, and both employ the spectral method. At convergence the two methods lead to the same results (Gauss's law). It seems possible that there is some correspondence between the iteration process in BCSA and the functional minimization process, which is analyzed below.

In Wang's model [29], the free energy functional of a heterogeneous system (without considering free charge) is formulated as

$$F=\int \frac{P^2(\mathbf{r})}{2\varepsilon_0\chi(\mathbf{r})}d^3r-\int \mathbf{E}^{ex}\cdot\mathbf{P}(\mathbf{r})d^3r+\frac{1}{2\varepsilon_0}\int \frac{d^3k}{(2\pi)^3}\left|\mathbf{n}\cdot\tilde{\mathbf{P}}(\mathbf{k})\right|^2 . \tag{A0}$$

This free energy functional is minimized through the time-dependent Ginzburg-Landau equation (TDGL), given by

$$\frac{\partial\mathbf{P}(\mathbf{r},t)}{\partial t}=-L\frac{\delta F}{\delta\mathbf{P}(\mathbf{r},t)} , \tag{A0}$$

where L is a positive kinetic coefficient. The $\delta F/\delta\mathbf{P}$ term can be explicitly written as

$$\frac{\delta F}{\delta \mathbf{P}(\mathbf{r},t)} = \frac{\mathbf{P}(\mathbf{r},t)}{\varepsilon_0 \chi(\mathbf{r})} - \mathbf{E}(\mathbf{r},t), \tag{A0}$$

where

$$\mathbf{E}(\mathbf{r},t) = \mathbf{E}^{ex} - \frac{1}{\varepsilon_0}\int \frac{d^3k}{(2\pi)^3}[\mathbf{n}\cdot\tilde{\mathbf{P}}(\mathbf{k},t)]\mathbf{n}e^{i\mathbf{k}\cdot\mathbf{r}} \tag{A0}$$

is the local electric field. Equation (A20) is consistent with Eq. (5) as ρ_f is zero since $\tilde{\rho}_b = -i\mathbf{k}\cdot\tilde{\mathbf{P}}$. Note that minimization of the functional ($\delta F / \delta \mathbf{P} = 0$) also leads to $\mathbf{P} = \varepsilon_0 \chi \mathbf{E}$ which is Eq. (4). From Eq. (A18), with time increment Δt the variation of polarization density is

$$\delta \mathbf{P}(\mathbf{r},t) = -(L\cdot\Delta t)\frac{\delta F}{\delta \mathbf{P}(\mathbf{r},t)} \ . \tag{A0}$$

By functional Taylor expansion, if $\delta \mathbf{P}$ is sufficiently small (as long as $L\cdot\Delta t$ is sufficient small) one may neglect higher order terms so that the variation of total free energy is correspondingly,

$$\delta F \approx \int \delta \mathbf{P}(\mathbf{r},t)\cdot\left(\frac{\delta F}{\delta \mathbf{P}(\mathbf{r},t)}\right)d^3r = \int -(L\cdot\Delta t)\left|\frac{\delta F}{\delta \mathbf{P}(\mathbf{r},t)}\right|^2 d^3r < 0. \tag{A0}$$

Therefore, the total free energy is guaranteed to monotonically decrease, provided that $L\cdot\Delta t$ is sufficiently small. This is the reason that in common phase-field models where TDGL (or the Allen-Cahn equation) is employed, the time increment usually needs to be sufficiently small (this is, however, not explicitly mentioned in [29]). Now if a gradient operator is applied to both sides of Eq. (A18) one obtains

$$\frac{\partial[\nabla\cdot\mathbf{P}(\mathbf{r},t)]}{\partial t} = -L\left[\frac{1}{\varepsilon_0}\nabla\cdot\left(\frac{\mathbf{P}(\mathbf{r},t)}{\chi(\mathbf{r})}\right) - \nabla\cdot\mathbf{E}(\mathbf{r},t)\right]. \tag{A0}$$

By using Eqs. (2-4) and assuming $\rho_f = 0$, we reach

$$\frac{\partial \rho_b(\mathbf{r},t)}{\partial t} = \frac{-L}{\varepsilon_0\chi(\mathbf{r})}\left[\varepsilon_0\mathbf{E}(\mathbf{r},t)\cdot\nabla\chi(\mathbf{r}) + \left(\chi(\mathbf{r})+1\right)\rho_b(\mathbf{r},t)\right]. \tag{A0}$$

Comparing Eq. (A24) with Eq. (10) one finds that if the coefficient λ in Step (d) of Algorithm 1 is set as $\lambda(\mathbf{r}) = L\cdot\Delta t / \varepsilon_0\chi(\mathbf{r})$, then the iteration process in BCSA is equivalent to the time

discretization of Eq. (A24). In that situation the BCSA algorithm can be considered as an extension of Wang's method. We verified that a position dependent $\lambda(\mathbf{r}) = L/\varepsilon_0\chi(\mathbf{r})$ indeed works for the BCSA algorithm if L is sufficiently small and $\chi(\mathbf{r})$ does not have zero value anywhere since $\chi(\mathbf{r})$ appears in the denominator position in Eqs. (A17) and (A19). However, in that situation the algorithm is much less efficient and the iteration number is not generally predictable.

We have also directly applied Wang's method (where the TDGL equation, Eq. (A18), is used) to the simulation of depolarization factor of a circular particle (cf. Fig. 2, the permittivity ratio is set to 20/2) with $L \cdot \Delta t / \varepsilon_0$ chosen to be 0.01 (The choices of L and Δt are, however, not specified in [29]). For comparison we have applied the BCSA algorithm to solve the same problem. With the same target precision the two simulation results are virtually the same except that the number of time steps required in TDGL is about two orders of magnitude higher than the number of iterations required in BCSA (the computational cost of one time step in Wang's method is comparable to that of one iteration in BCSA). When both the methods are applied to the complex case in Fig. 4, again, the simulation results are virtually the same but the efficiency of BCSA algorithm is about two orders of magnitude higher.

Finally, we note that it is possible to optimize the efficiency of the TDGL-based algorithm in [29] in terms of the coefficients L and Δt. Since for solving electrostatic problems, the time in TDGL is not physical and in principle whether the system 'free energy' monotonically decreases is not a must for solving static problems, we have tried to discard the 'rule of thumb' that $L \cdot \Delta t$ needs to be sufficiently small and instead, used computer to test the optimal $L \cdot \Delta t$ by exhaustively exploring the parameter space. For the particular case in Fig. 2, the optimal $L \cdot \Delta t / \varepsilon_0$ is found to be, surprisingly, as large as 0.95. By using this optimal value for this specific case the number of time steps required in TDGL approaches the iteration number in BCSA (In our preliminary tests, for several cases the computational efficiency of the BCSA algorithm appears to represent the upper limit for the TDGL-based algorithm with the optimal $L \cdot \Delta t$). It might be nontrivial to theoretically justify using such as a large value of $L \cdot \Delta t$ in TDGL, and unfortunately, $L \cdot \Delta t = 0.95$ is found to be not generally valid. Therefore, at this

point for general cases $L \cdot \Delta t$ in the TDGL equation yet has to be set small, and in that situation the efficiency of the TDGL-based algorithm is much lower than BCSA in general for solving electrostatic problems and the time steps required in the TDGL-based algorithm is generally not predictable. It is possible to further explore the optimization method for the kinetic coefficients in the TDGL equation for solving static heterogeneity problems, which is however beyond the scope of this paper.

*E-mail: tianle.cheng@contr.netl.doe.gov; youhai.wen@netl.doe.gov

Acknowledgement

The authors are grateful to Prof. Yu U. Wang and Prof. Yongmei M. Jin (both in Michigan Technological University) for valuable discussions, and Dr. Dan Sorescu and Dr. Jeffrey A. Hawk for critically reading the manuscript. We also thank the Strategic Center for Coal, Cross-Cutting Research, Dr. Susan Maley, Technology Manager, for supporting this NETL/ORD activity through the IPT project led by Dr. David E. Alman. T.-L.C. acknowledges the Postgraduate Research Program operated by Oak Ridge Institute for Science and Education (ORISE) and the Extreme Science and Engineering Discovery Environment (XSEDE) that is supported by National Science Foundation grant number OCI-1053575. This report was prepared as an account of work sponsored by an agency of the United States Government. Neither the United States Government nor any agency thereof, nor any of their employees, makes any warranty, express or implied, or assumes any legal liability or responsibility for the accuracy, completeness, or usefulness of any information, apparatus, product, or process disclosed, or represents that its use would not infringe privately owned rights. Reference herein to any specific commercial product, process, or service by trade name, trademark, manufacturer, or otherwise does not necessarily constitute or imply its endorsement, recommendation, or favoring by the United States Government or any agency thereof. The views and opinions of authors expressed herein do not necessarily state or reflect those of the United States Government or any agency thereof.

References

[1] C. Kittel, *Introduction to Solid State Physics, 7th ed.* (John Wiley & Sons, New York, NY, 1996).

[2] D. L. House, H. Luo, and S. Chang, J. Colloid Interface Sci. **374**, 141 (2012).

[3] H. M. Tian, J. Y. Shao, Y. C. Ding, X. M. Li, and H. Z. Liu, Langmuir **29**, 4703 (2013).

[4] R. Pethig, Biomicrofluidics **4**, 022811 (2010).

[5] C. Grosse, and A. V. Delgado, Curr. Opin. Colloid Interface Sci. **15**, 145 (2010).

[6] X. Y. Song, J. Chem. Phys. **116**, 9359 (2002).

[7] D. Voges, and A. Karshikoff, J. Chem. Phys. **108**, 2219 (1998).

[8] M. Schaefer, and M. Karplus, J. Phys. Chem. **100**, 1578 (1996).

[9] B. Honig, and A. Nicholls, Science **268**, 1144 (1995).

[10] A. Warshel, P. K. Sharma, M. Kato, and W. W. Parson, Biochimica Et Biophysica Acta-Proteins and Proteomics **1764**, 1647 (2006).

[11] L. Li, C. Li, Z. Zhang, and E. Alexov, J. Chem. Theory Comput. **9**, 2126 (2013).

[12] B. Sareni, L. Krahenbuhl, A. Beroual, and C. Brosseau, J. Appl. Phys. **81**, 2375 (1997).

[13] C. Brosseau, J. Phys. D-Appl. Phys. **39**, 1277 (2006).

[14] E. Tuncer, Y. V. Serdyuk, and S. M. Gubanski, IEEE Trns. Dielectr. Electr. Insul. **9**, 809 (2002).

[15] C. Brosseau, and A. Beroual, Prog. Mater. Sci. **48**, 373 (2003).

[16] A. Mejdoubi, and C. Brosseau, Physical Review E **74**, 031405 (2006).

[17] Y. H. Cheng, X. L. Chen, K. Wu, S. N. Wu, Y. Chen, and Y. M. Meng, J. Appl. Phys. **103**, 034111 (2008).

[18] L. Jylha, and A. H. Sihvola, IEEE Trans. Geosci. Remote Sensing **43**, 59 (2005).

[19] Z. M. Chen, Q. Du, and J. Zou, SIAM Journal on Numerical Analysis **37**, 1542 (2000).

[20] F. J. García de Abajo, and A. Howie, Phys. Rev. B **65**, 115418 (2002).

[21] H. Cheng, and S. Torquato, Phys. Rev. B **56**, 8060 (1997).

[22] P. K. Ghosh, and M. E. Azimi, IEEE Trns. Dielectr. Electr. Insul. **1**, 975 (1994).

[23] M. R. Hossan, R. Dillon, A. K. Roy, and P. Dutta, J. Colloid Interface Sci. **394**, 619 (2013).

[24] R. A. Marcus, J. Chem. Phys. **24**, 966 (1956).

[25] P. Attard, J. Chem. Phys. **119**, 1365 (2003).

[26] R. Allen, J. P. Hansen, and S. Melchionna, Phys. Chem. Chem. Phys. **3**, 4177 (2001).

[27] V. Jadhao, F. J. Solis, and M. O. de la Cruz, J. Chem. Phys. **138**, 054119 (2013).

[28] D. Boda, D. Gillespie, W. Nonner, D. Henderson, and B. Eisenberg, Physical Review E **69**, 046702 (2004).

[29] Y. U. Wang, Appl. Phys. Lett. **96** (2010).

[30] J. L. Wilson, P. Poddar, N. A. Frey, H. Srikanth, K. Mohomed, J. P. Harmon, S. Kotha, and J. Wachsmuth, J. Appl. Phys. **95**, 1439 (2004).

[31] J. D. Adams, U. Kim, and H. T. Soh, Proc. Natl. Acad. Sci. U. S. A. **105**, 18165 (2008).

[32] L. Q. Chen, Ann. Rev. Mater. Res. **32**, 113 (2002).

[33] H. Emmerich, Adv. Phys. **57**, 1 (2008).

[34] A. G. Khachaturyan, *Theory of structural transformations in solids* (Wiley, New York, 1983).

[35] P. C. Millett, and Y. U. Wang, Acta Mater. **57**, 3101 (2009).

[36] Y. M. M. Jin, Appl. Phys. Lett. **103**, 021906 (2013).

[37] J. W. Cahn, and J. E. Hilliard, J. Chem. Phys. **28**, 258 (1958).

[38] J. A. Osborn, Physical Reivew **67**, 351 (1945).

[39] Y. U. Wang, D. Q. Tan, and J. Krahn, J. Appl. Phys. **110**, 044103 (2011).

[40] J. E. Guyer, W. J. Boettinger, J. A. Warren, and G. B. McFadden, Physical Review E **69**, 021604 (2004).

[41] Y. U. Wang, Acta Mater. **55**, 3835 (2007).

[42] T.-L. Cheng, and Y. U. Wang, J. Colloid Interface Sci. **402**, 267 (2013).

[43] J. Happel, and H. Brenner, *Low Reynolds number hydrodynamics with special applications to particulate media* (Noordhoff International Publishing, Leyden, The Netherlands, 1973).

[44] J. F. Brady, and G. Bossis, Annual Review of Fluid Mechanics **20**, 111 (1988).

[45] B. Cichocki, B. U. Felderhof, K. Hinsen, E. Wajnryb, and J. Blawzdziewicz, J. Chem. Phys. **100**, 3780 (1994).

[46] J. G. Kirkwood, and J. Riseman, J. Chem. Phys. **16**, 565 (1948).

[47] E. Kim, K. Stratford, and M. E. Cates, Langmuir **26**, 7928 (2010).

[48] T.-L. Cheng, Y.-H. Wen, and J. A. Hawk, J. Phys. Chem. C **118**, 1269 (2014).

[49] T.-L. Cheng, and Y.-H. Wen, Journal of Physical Chemistry Letters **5**, 2289 (2014).

[50] Y. M. M. Jin, Acta Mater. **57**, 2488 (2009).

[51] T. L. Cheng, Y. X. Y. Huang, C. M. Rogers, and Y. M. M. Jin, J. Appl. Phys. **107** (2010).

[52] A. Hubert, and R. Schäfer, *Magnetic domains, the analysis of magnetic microstructures* (Springer-Verlag, Berlin, 1998).

[53] J. E. Guyer, W. J. Boettinger, J. A. Warren, and G. B. McFadden, Physical Review E **69**, 021603 (2004).